A&A 462, 525–533 (2007)
DOI: 10.1051/0004-6361:20065429

Astronomy & Astrophysics

The host galaxies of radio-quiet quasars at $0.5 < z < 1.0$⋆,⋆⋆

T. Hyvönen[1], J. K. Kotilainen[1], E. Örndahl[1], R. Falomo[2], and M. Uslenghi[3]

[1] Tuorla Observatory, University of Turku, Väisäläntie 20, 21500 Piikkiö, Finland
e-mail: [totahy;jarkot]@utu.fi;orndahl@gmail.com
[2] INAF - Osservatorio Astronomico di Padova, Vicolo dell'Osservatorio 5, 35122 Padova, Italy
e-mail: falomo@pd.astro.it
[3] INAF - IASF Milano, Via E. Bassini 15, 20133 Milano, Italy
e-mail: uslenghi@mi.iasf.cnr.it

Received 13 April 2006 / Accepted 27 September 2006

ABSTRACT

We present near-infrared H-band imaging of 15 intermediate redshift ($0.5 < z < 1$) radio quiet quasars (RQQ) to characterize the properties of their host galaxies. We are able to clearly detect the surrounding nebulosity in 12 objects, whereas the object remains unresolved in three cases. For all the resolved objects, we find that the host galaxy is well represented by a de Vaucouleurs $r^{1/4}$ surface brightness law. This is the first reasonably sized sample of intermediate redshift RQQs studied in the near-infrared.
The RQQ host galaxies are luminous (average $M_{\rm H} = -26.3 \pm 0.6$) and large giant elliptical galaxies (average bulge scale length $R_{\rm e} = 11.3 \pm 5.8$ kpc). RQQ hosts are ∼1 mag brighter than the typical low redshift galaxy luminosity L^*, and their sizes are similar to those of galaxies hosting lower redshift RQQs, indicating that there is no significant evolution at least up to $z \sim 1$ of the host galaxy structure. We also find that RQQ hosts are ∼0.5−1 mag fainter than radio-loud quasar (RLQ) hosts at the similar redshift range. The comparison of the host luminosity of intermediate redshift RQQ hosts with that for lower z sources shows a trend that is consistent with that expected from the passive evolution of the stars in the host galaxies. The nuclear luminosity and the nucleus/host galaxy luminosity ratio of the objects in our sample are intermediate between those of lower redshift RQQs and those of higher redshift ($z > 1$) RQQs.

Key words. galaxies: quasars: general – galaxies: active – galaxies: elliptical and lenticular, cD – galaxies: nuclei – galaxies: photometry – infrared: galaxies

1. Introduction

To understand the quasar phenomenon, and AGN in general, it is important to study their orientation-independent properties, such as the luminosity of their host galaxies and their large-scale environment. The relationship between quasars and their host galaxies, in particular, is a key ingredient for understanding the quasar activity, the formation of galaxies, and the strong cosmological evolution of the space density of the quasar population (Warren et al. 1994). The shape of this evolution as a function of z is similar to that of the black hole (BH) mass accretion rate and the cosmic star formation history of the Universe (Madau et al. 1998; Franceschini et al. 1999; Chary & Elbaz 2001; Barger et al. 2001; Yu & Tremaine 2002; Marconi et al. 2004), suggesting a fundamental relationship between the processes of the formation of massive galaxy bulges and their nuclei. Thus, studies of quasars and their host galaxies will give us a more detailed understanding of galaxy evolution. According to the hierarchical model of structure formation (Kauffmann & Hähnelt 2000; Di Matteo et al. 2003), there should be a correlation between the evolution of massive spheroids and the processes that fuel their central BHs.

Inactive supermassive BHs are prevalent in nearby inactive massive spheroids (e.g., Ferrarese 2002; Barth 2004). Recently, at low redshift, correlations have been found between the BH mass, and the luminosity and the central stellar velocity dispersion of the host galaxy bulge (e.g., Magorrian et al. 1998; van der Marel 1999; Gebhardt et al. 2000; Ferrarese & Merritt 2000; McLure & Dunlop 2002; Marconi & Hunt 2003; Bettoni et al. 2003; Häring & Rix 2004). These findings suggest that nuclear activity is a common phenomenon during the lifetime of a massive galaxy with recurrent accretion episodes, and that the nuclear power depends on the mass of the galaxy.

Imaging of quasar host galaxies from space (e.g., HST) has the advantage over ground-based observations of having an excellent spatial resolution (narrow PSF) to resolve the host galaxy close to the nucleus. However, HST has a relatively small aperture that translates into a limited capability to detect faint extended nebulosity. A number of ground-based (e.g., McLeod & Rieke 1994a,b; Percival et al. 2001) and space-based (e.g., Bahcall et al. 1997; Hamilton et al. 2002; Dunlop et al. 2003; Pagani et al. 2003; Floyd et al. 2004) optical and near-infrared (NIR) studies of low redshift quasar hosts ($z < 0.5$) have shown that both radio-quiet (RQQ) and radio-loud (RLQ) quasars are predominantly hosted by luminous, massive elliptical galaxies that are typically brighter than L^* galaxies (the Schechter function's characteristic luminosity) and as bright as low redshift radio galaxies (RG). Some of these studies also suggest that the morphology of the host may depend on the nuclear luminosity in the sense that high luminosity RQQs are exclusively hosted in

⋆ Based on observations made with the Nordic Optical Telescope, operated on the island of La Palma jointly by Denmark, Finland, Iceland, Norway, and Sweden, in the Spanish Observatorio del Roque de los Muchachos of the Instituto de Astrofísica de Canarias.
⋆⋆ Figure 2 is only available in electronic form at http://www.aanda.org

elliptical galaxies (or dominated by the spheroidal component), while low luminosity RQQ can also be located in early-type spiral (disk-dominated) galaxies (Hamilton et al. 2002; Dunlop et al. 2003).

To investigate the evolution of quasar host galaxies as a function of cosmic time, observations are needed over a large redshift range. Unfortunately, high redshift ($z > 0.5$) hosts have, until recently, been relatively little studied because of difficulties due to limited spatial resolution and the high nucleus/host luminosity contrast (caused by $(1 + z)^4$ cosmological surface brightness dimming). In fact, although a number of detections of quasar hosts at $z > 1$ based on ground-based (e.g., Falomo et al. 2001, 2004, 2006; Kotilainen et al. 2006) and space observations (e.g., Kukula et al. 2001; Peng et al. 2006) are available, the only systematic observations of large samples at intermediate redshift ($0.5 < z < 1$) in the NIR have been made by Kotilainen et al. (1998) and Kotilainen & Falomo (2000) (hereafter K98 and K00, respectively) for a total sample of ∼40 flat and steep spectrum RLQs (FSRQ and SSRQ, respectively). In particular, no homogenous studies of matched samples of RLQs and RQQs at intermediate redshift have yet been made. Such a sample would allow us to study and compare the evolution of the hosts of both types of quasars.

The classes of RLQs and RQQs differ in their radio properties, but they also appear to be different in their host galaxy luminosity (Dunlop et al. 2003; Floyd et al. 2004; Falomo et al. 2004, K98; K00), in the sense that RLQ hosts are significantly more luminous than RQQ hosts at all redshifts in the redshift range $0 < z < 2$. In addition, both types of quasars follow the passive evolution of massive elliptical galaxies. This is inconsistent with models of hierarchical galaxy formation (Kauffmann & Hähnelt 2000; Di Matteo et al. 2003), which predict a decrease in the luminosity (mass) of the galaxies at high redshift, followed by an increase toward the present epoch due to galactic mergers.

We present here a deep high spatial resolution NIR H-band imaging study of the host galaxies of a sizeable sample of RQQs at intermediate redshift. For all the RQQs in the sample, these are the first high quality NIR imaging observations, and the first detection of the host galaxies. The RQQ sample was extracted from the quasar catalog of Veron-Cetty & Veron (2003) as having $0.5 < z < 1$, $-24 < M_B < -28$, and no radio emission listed in that catalog or in the catalog of the FIRST 1.4 GHz survey (Becker et al. 1997). All selected targets were also required to have at least one sufficiently bright field star within 2 arcmin distance from the quasar, to allow a reliable characterization of the PSF. In total, 15 RQQs were observed. Figure 1 shows their distribution in the $z - M_B$ plane, compared to the FSRQ and SSRQ samples (K98; K00). The average redshift and the absolute magnitude of the RQQ sample are $z = 0.728 \pm 0.138$ and $M_B = -25.8 \pm 0.9$, respectively. For the combined sample of FSRQs and SSRQs from K98 and K00, the corresponding average values are $z = 0.719 \pm 0.138$ and $M_B = -25.7 \pm 1.0$. The RQQ sample is thus well matched with the FSRQs and SSRQs samples in both redshift and absolute magnitude, allowing us to homogeneously compare the properties of RQQs and RLQs in this redshift range. The general properties of the observed objects are given in Table 1.

The immediate objective of this study is to resolve the host galaxies of the quasars and to derive their global properties: e.g., absolute magnitude, effective radius, central surface brightness, and the nucleus/host galaxy luminosity ratio. These properties will allow us to assess the luminosity gap between the RLQ and RQQ hosts at intermediate redshift and to investigate in more detail the cosmological evolution of both types of quasars

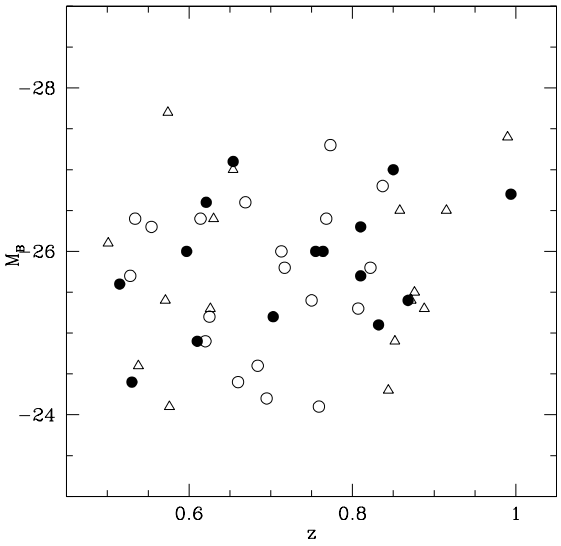

Fig. 1. The absolute B-band magnitude (Veron-Cetty & Veron 2003) of the intermediate redshift RQQs and RLQs versus redshift. RQQs from this work are marked as filled circles, SSRQs from K00 as open circles, and FSRQs from K98 as open triangles.

Table 1. The sample and the journal of observations[a].

Name	z	V	M_B	Date	T_{exp} min	Seeing arcsec	ε
(1)	(2)	(3)	(4)	(5)	(6)	(7)	(8)
HS 0010+3611	0.530	18.2	−24.4	27/08/2004	45	0.80	0.05
1E 0112+3256	0.764	18.9	−26.0	27/08/2004	55	0.80	0.22
PB 6708	0.868	18.6	−26.6	24/01/2005	64	0.95	0.08
KUV 03086-0447	0.755	17.5	−25.7	23/01/2005	106	0.95	0.03
US 3828	0.515	16.9	−25.1	22/01/2005	92	0.95	0.06
MS 08287+6614	0.610	18.0	−26.3	23/01/2005	73	0.85	0.10
TON 392	0.654	16.0	−25.6	24/01/2005	44	1.00	0.11
US 971	0.703	18.1	−27.1	22/01/2005	61	0.80	0.07
HE 0955-0009	0.597	16.9	−25.4	23/01/2005	104	0.90	0.04
HE 1100-1109	0.994	17.5	−25.2	22/01/2005	73	0.90	0.10
CSO 769	0.850	16.9	−24.4	23/01/2005	53	0.85	0.15
HS 1623+7313	0.621	16.3	−27.0	28/08/2004	75	0.85	0.04
HS 2138+1313	0.810	18.1	−24.9	28/08/2004	60	1.00	0.16
LBQS 2249-0154	0.832	18.7	−26.0	28/08/2004	64	0.90	0.10
ZC 2351+010B	0.810	17.5	−26.7	28/08/2004	40	1.00	0.16

[a] Column (1) gives the name of the object; (2) the redshift; (3) the V-band apparent magnitude; (4) the B-band absolute magnitude; (5) the date of observation; (6) total exposure time; (7) seeing $FWHM$ (arcsec); and (8) the average ellipticity of the field stars.

between the peak of the quasar activity ($z \sim 2$–3) and the present epoch. The determination of the RQQ host properties in the redshift gap $0.5 < z < 1$ is an important contribution for the study of the behavior of the RQQ host luminosity as a function of cosmic time. At lower redshift, volume selection effects are more severe and current samples of resolved RQQ are rather poorly defined. In addition, we shall investigate the dependence of the host galaxy properties on the nuclear luminosity in our quasar sample and also compare the occurrence of close companions between RLQs and RQQs, as well as in comparison to lower and higher redshifts, to assess the importance of interactions for the triggering and fueling of quasar activity.

The outline of the paper is as follows. In Sect. 2, we describe the observations, data reduction, and the method of the analysis. In Sect. 3, we present the results and discussion concerning the host galaxy properties, the nuclear component and the close

environment of the RQQs. Finally, summary and main conclusions are given in Sect. 4. Throughout this paper, to facilitate comparison with the FSRQs and SSRQs, $H_0 = 50\,\mathrm{km\,s^{-1}\,Mpc^{-1}}$ and $q_0 = 0$ cosmology is used. The conclusions do not change significantly if the concordant Λ-cosmology is used.

2. Observations, data reduction, and analysis

The observations were carried out during two observing runs in August 2004 and January 2005 at the 2.5 m Nordic Optical Telescope (NOT). We used the 1024×1024 pixel NOTCam NIR detector with a pixel scale of $0\farcs235$ pixel^{-1}, giving a field of view of $\sim 4 \times 4$ arcmin^2. The H-band (1.65 μm), corresponding to $\sim 0.8-1.1$ μm rest-frame wavelength, was used for all the observations. This filter choice minimizes the nucleus/host brightness contrast, while the extinction, the K-correction, and the contribution from quasar emission lines and scattered nuclear light are insignificant. In addition, these observations can be directly compared with our previous FSRQ and SSRQ data. The seeing during the observations, as derived from the median *FWHM* size of the stars in each frame, ranged from $0\farcs75$ to $1\farcs00$ arcsec *FWHM* (mean and median $0\farcs9$ *FWHM*). A journal of the observations is given in Table 1. The images were acquired by dithering the targets across the array in a random grid within a box of about 20 arcsec, and taking a 60 s exposure at each position, always keeping the target well inside the field. Individual exposures were then coadded to achieve the final integration time for each object (Table 1).

2.1. Data reduction

Data reduction was performed using IRAF[1] and closely follows the method presented in Kotilainen et al. (2005). Bad pixels were corrected for in each image using a mask made from the ratio of two sky flats with different illumination levels. Sky subtraction was performed for each science image using a median averaged frame of all the other temporally close frames in a grid of eight exposures. Flat fielding was made using normalized median averaged twilight sky frames with different illumination levels. Finally, images of the same target were aligned to subpixel accuracy using field stars as reference points and combined after removing spurious pixel values to obtain the final reduced co-added image. Standard stars from Hunt et al. (1998) were observed throughout the nights to provide photometric calibration, which resulted in internal photometric accuracy of ~ 0.1 mag, as determined from the comparison of all observed standard stars.

2.2. 2 D analysis

Two-dimensional analysis was carried out using AIDA (Astronomical Image Decomposition and Analysis, Uslenghi & Falomo, in prep.), a software package specifically designed to perform two-dimensional model fitting of quasar images, providing simultaneous decomposition into nuclear and host components. The analysis consists of two main parts: a) PSF modeling and b) quasar host characterization.

[1] IRAF is distributed by the National Optical Astronomy Observatories, which are operated by the Association of Universities for Research in Astronomy, Inc., under cooperative agreement with the National Science Foundation.

2.2.1. PSF modeling

To detect the host galaxies of quasars and to characterize their properties, the key factors are the nucleus-to-host luminosity ratio and the seeing (the shape of the PSF). The most critical part of the analysis is thus to perform a detailed study of the PSF for each frame. The PSF modeling is based on fitting a parameterized bidimensional model to the stars.

For PSF modeling, the point-like objects of the image were classified as stars based on their *FWHM*, sharpness, and roundness. When possible, a sufficiently bright, saturated star was included in the list of reference stars to model the shape of the PSF wings, against which most of the signal from the surrounding nebulosity will be detected. The relatively large field of view of NOTCam ($\sim 4 \times 4$ arcmin^2) and the constraint on the quasar selection to have at least one bright star within 2 arcmin from the quasar allowed us to reach this goal and thus to perform a reliable characterization of the PSF. Images with a large number of stars distributed over the field of view have been checked to account for any possible positional dependence of the PSF. No significant variations were found and in this analysis the PSF has been assumed to be spatially invariant, i.e., the same model has been fitted simultaneously to all the reference stars of the image.

For each star, a mask was created to exclude contamination from nearby sources, bad pixels, and other defects affecting the image. Then the local background was computed in a circular annulus centered on the source, with the MMM algorithm (from IDL Astrolib). Its uncertainty was estimated from the standard deviation of the values computed in sectors of concentric subannuli included in this area. The region to be used in the fit was selected by defining an inner and outer radius of a circular area. The inner radius was set to zero, except for bright saturated stars, thus allowing their core to be excluded from the fitting. The outer radius was generally set to correspond to a distance where the signal in the radial profile was not significantly higher than the noise.

Stellar images were found to be slightly elliptical, with FWHM varying from 0.80 to 1.05 arcsec and the average ellipticity at half maximum $\varepsilon \sim 0.15$. Characteristic average values for the stars in each quasar image are presented in Table 1. As stated above, the goodness of the model is strictly related to the availability of suitable stars in the images. Only six images contain a bright enough star to model the PSF wings at radius $\geq$3 arcsec. However, for all the images we were able to extract a PSF model up to the maximum radius where the signal from the quasar was present. The worst case in this respect is ZC2351+010B, with only one star available due to the highly irregular background and the presence of image defects that prevented the use of the only bright star in the field.

2.2.2. Quasar host characterization

Once a suitable representation of the PSF was determined, the quasar images (prepared in an identical way to that described for the stars in the previous section) were first fitted with only the PSF model to provide a first order indication of a deviation from the PSF shape. If the residuals did not reveal any systematic excess, the object was considered unresolved. Otherwise, the object was fitted with a scaled PSF to represent the nucleus, and a de Vaucouleurs $r^{1/4}$ model or an exponential disk model convolved with the PSF to represent the host galaxy, using an iterative least-squares fit to the observed data.

With the applied procedure we have derived the luminosity and the scale length of the host galaxies and the luminosity of the

Table 2. Properties of the host galaxies[a].

Name	z	$K-$corr	$m_{\rm H,nuc}$	$m_{\rm H,host}$	$\mu_{\rm e}^{b}$	$r_{\rm e}$	$R_{\rm e}$	$M_{\rm H,nuc}^{c}$	$M_{\rm H,host}^{d}$	$L_{\rm nuc}/L_{\rm host}$	Note	$\chi^2_{\rm psf+gal}/\chi^2_{\rm psf}$
		mag	mag	mag	mag	arcsec	kpc	mag	mag			
(1)	(2)	(3)	(4)	(5)	(6)	(7)	(8)	(9)	(10)	(11)	(12)	(13)
HS 0010+3611	0.530	0.12	15.03	17.26	14.68	1.3 ± 0.6	10.5 ± 5.0	-28.0	-25.9 ± 0.3	7.8	R	0.93
1E 0112+3256	0.764	0.18	17.94	18.18	15.46	0.9 ± 0.5	8.9 ± 4.9	-26.1	-26.0 ± 0.3	1.25	R	0.70
PB 6708	0.868	0.22	17.13	>18.50				-27.2	>-26.1	>3.5	U	
KUV 03086-0447	0.755	0.17	15.16	17.14	14.61	1.0 ± 0.5	9.7 ± 4.9	-28.8	-27.0 ± 0.3	6.2	R	0.63
US 3828	0.515	0.11	15.70	17.28	14.52	1.2 ± 0.5	9.8 ± 4.1	-27.3	-25.8 ± 0.3	6.9	R	0.85
MS 08287+6614	0.610	0.13	16.45	17.42	13.97	0.8 ± 0.4	6.9 ± 3.6	-27.0	-26.1 ± 0.2	2.4	R	0.65
TON 392	0.654	0.14	14.41	17.07	14.23	1.0 ± 0.4	8.9 ± 3.7	-29.2	-26.6 ± 0.3	11.6	R	0.93
US 971	0.703	0.15	16.57	18.27	15.78	1.1 ± 0.6	10.1 ± 5.7	-27.2	-25.7 ± 0.2	4.8	R	0.94
HE 0955-0009	0.597	0.13	15.18	>17.20				-28.2	>-26.3	>6.4	U	
HE 1100-1109	0.994	0.30	15.23	17.93	17.99	2.5 ± 0.7	27.3 ± 7.6	-29.5	-27.1 ± 0.2	12.0	R	0.86
CSO 769	0.850	0.22	16.42	17.99	16.19	1.2 ± 0.5	13.4 ± 5.1	-27.9	-26.5 ± 0.3	4.2	R	0.98
HS 1623+7313	0.621	0.14	15.86	18.18	15.68	1.2 ± 0.5	10.5 ± 4.5	-27.6	-25.4 ± 0.2	8.5	R	0.86
HS 2138+1313	0.810	0.20	15.57	>18.00				-28.6	>-26.4	>9.4	U	
LBQS 2249-0154	0.832	0.21	16.38	17.43	14.36	0.7 ± 0.3	7.1 ± 3.1	-27.9	-27.0 ± 0.5	2.6	R	0.67
ZC 2351+010B	0.810	0.20	16.86	18.52	16.59	1.2 ± 0.6	12.3 ± 6.1	-27.3	-25.9 ± 0.6	4.6	R	0.92

[a] Columns (1) and (2) give the name and the redshift of the object; (3) the $K-$correction for first-ranked elliptical galaxies from Neugebauer et al. (1985), interpolated to the redshifts of the RQQs; (4) and (5) the apparent H-band nuclear and host galaxy magnitude; (6) the effective surface brightness $\mu_{\rm e}$; (7) and (8) the bulge scale-length in arcsec and kpc; (9) and (10) the absolute H-band nuclear and host galaxy magnitude; (11) the nucleus/host galaxy luminosity ratio; (12) R = resolved, U = unresolved; and (13) the ratio of the $\chi^2_{\rm psf+gal}$ and $\chi^2_{\rm psf}$. [b] Corrected for cosmological dimming. [c] The RQQ nuclei are assumed to have power-law spectra with $\alpha \sim -1$ and therefore to have negligible $K-$correction. [d] Corrected for $K-$correction.

nuclei. An estimate of the errors associated with the computed parameters was obtained by a Monte Carlo simulation of synthetic data sets. Simulated quasar images were generated adding noise to the best-fit model, then the fit procedure was applied to these images, producing a "best-fit" combination of parameters for each image. For each parameter, the standard deviation of the best-fit values gives an estimate of the uncertainty on the parameters under the assumption that the distribution of the errors does not vary rapidly as a function of the values of the parameters. Obviously, this procedure does not take into account systematic errors generated by an imperfect modeling of the PSF, which can be roughly estimated by comparing the results obtained with different PSF models, statistically consistent with the available data. For our worst case, ZC2351+0108, for example, this effect produces an uncertainty of ∼0.6 mag for the brightness of the host galaxy. Instead, in images that have several suitable reference stars (e.g., TON 392), the uncertainty is dominated by the noise. Upper limits to the host magnitudes for unresolved objects were computed by adding a galaxy component to the PSF and varying its surface brightness until the model profile was no longer consistent with the object profile.

While the total magnitude of the host galaxy can be derived with a typical internal error of 0.2−0.6 mag (0.3 mag on average), the scale length is often poorly constrained. This depends on the degeneracy that occurs between the effective radius $r_{\rm e}$ and the surface brightness $\mu_{\rm e}$. Estimated errors of the effective radius and host galaxy magnitude for each target are given in Table 2. No correlation is apparent between $r_{\rm e}$ and seeing or nuclear magnitude.

At these relatively high redshifts, it is difficult to distinguish between the exponential disk and the bulge ($r^{1/4}$ law) models for the host galaxy from the luminosity distributions. However, in all cases a bulge model resulted in a better fit (lower χ^2 value) than a disk model, and in what follows, we have assumed that the host galaxies can be represented as elliptical galaxies following a de Vaucouleurs model. This is supported by the strong evidence at low redshift for the predominance of bulge dominated hosts of quasars (Hamilton et al. 2002; Dunlop et al. 2003; Pagani et al. 2003). Note that adopting a disk model instead would result in fainter host galaxies, by ∼0.5 mag on average, but this would introduce no systematic differences to our conclusions.

3. Results and discussion

In Fig. 2 we show H-band contour plots for the quasars, the PSF model subtracted image of the host galaxy, the residuals after the model fitting, and the radial surface brightness profiles with the best-fit model from the procedure described in the previous section. We were able to find significant deviations of the radial profile with respect to its PSF, and thus clearly detect the host galaxy in 12 objects, whereas the host galaxy remained unresolved in three objects. The nuclear and host galaxy magnitudes, and the effective radii of the host galaxies are summarized in Table 2. The absolute magnitudes of the host galaxies have been K-corrected using the optical-NIR evolutionary synthesis model for elliptical galaxies (Neugebauer et al. 1985). The size of this correction is $m_{\rm H} \sim 0.16$ at the average redshift of the RQQ sample, $z \sim 0.73$ (see Table 2). No $K-$correction was applied to the nuclear component, which was assumed to have a power-law spectrum ($f_\nu \propto \nu^{-\alpha}$) with $\alpha \sim -1$. No correction for Galactic extinction was applied since it is negligible in the observed H-band.

Because of the three upper limits in our sample, we used the statistical survival analysis method for right censored data (Feigelson & Nelson 1985) to estimate the mean value μ of the luminosity of the host galaxies. We used

$$\mu = \sum_{j=1}^{r+1} S\,[x_j][x_j - x_{j+1}]$$

where $S\,[x_j]$ is the Kaplan–Meier estimator, x_j is each value of the sample, and x_r is the maximum value of the sample. The variance was also estimated using the method in Feigelson & Nelson (1985), but its contribution to the error is insignificant.

Table 3. Comparison of average host galaxy properties with other RQQ samples[a].

Sample	Filter	N	$\langle z \rangle$	M_B	$\langle M_{H,nuc} \rangle^c$	$\langle M_{H,host} \rangle^c$
(1)	(2)	(3)	(4)	(5)	(6)	(7)
RQQ (this work)	H	12	0.720 ± 0.142	−25.8 ± 0.9	−27.8 ± 1.1	−26.3 ± 0.6
RQQ/R+U[b] (this work)	H	15	0.728 ± 0.138	−25.8 ± 0.9	−27.9 ± 1.0	−26.2 ± 0.6
RQQ (McLeod & Rieke 1994a)	H	22/24	0.103 ± 0.029		−25.1 ± 0.5	−24.9 ± 0.6
RQQ (Taylor et al. 1996)	K	19/19	0.157 ± 0.062	−23.8 ± 0.6	−26.1 ± 0.9	−25.7 ± 0.7
RQQ (Dunlop et al. 2003)	R	13/13	0.175 ± 0.01		−24.3 ± 0.6	−25.9 ± 0.2
RQQ (Bahcall et al. 1997)	V	14/14	0.183 ± 0.046	−24.9 ± 0.5		−25.1 ± 0.6
RQQ (McLeod & Rieke 1994b)	H	18/20	0.196 ± 0.047		−26.5 ± 0.9	−25.7 ± 0.6
RQQ (Percival et al. 2001)	K	12/14	0.362 ± 0.061	−25.6 ± 0.8	−27.4 ± 0.9	−25.0 ± 0.4
RQQ (Floyd et al. 2004)	V	10/10	0.390 ± 0.031		−26.2 ± 1.5	−26.3 ± 0.3
RQQ (Hooper et al. 1997)	R	10/10	0.433 ± 0.032		−25.8 ± 0.8	−25.6 ± 0.5
RQQ (Kukula et al. 2001)	J	4/5	0.931 ± 0.038		−25.4 ± 0.9	−26.1 ± 0.5
RQQ (Falomo et al. 2004)	H/K	6/7	1.519 ± 0.165	−26.7 ± 0.8	−29.2 ± 1.2	−26.6 ± 0.2
RQQ (Peng et al. 2006)	H	14/14	1.54 ± 0.21		−27.9 ± 1.2	−26.1 ± 0.8
RQQ (Kotilainen et al. 2006)	H/K	6/6	1.56 ± 0.25	−25.5 ± 0.5	−27.3 ± 0.5	−26.6 ± 0.9
RQQ (Kukula et al. 2001)	H	5/5	1.856 ± 0.120		−27.3 ± 0.5	−26.6 ± 0.9
L^* (Mobasher et al. 1993)	K	136	0.077 ± 0.030			−25.0 ± 0.2
BCG (Thuan & Puschell 1989)	H	84	0.074 ± 0.026			−26.3 ± 0.3
BCG (Aragon-Salamanca et al. 1998)	K	25	0.449 ± 0.266			−27.0 ± 0.3
FSRQ (Kotilainen et al. 1998)	H	9/16	0.671 ± 0.157	−26.2 ± 1.1	−29.7 ± 0.8	−26.7 ± 1.2
SSRQ (Kotilainen & Falomo 2000)	H	16/19	0.690 ± 0.088	−25.6 ± 1.0	−28.3 ± 1.3	−27.0 ± 1.2

[a] Column (1) gives the sample; (2) the filter; (3) the resolved/total number of objects in the sample; (4) the average redshift of the sample; (5) the absolute B-band magnitude of the quasar, and (6) and (7) the average H-band nuclear and host galaxy absolute magnitude of the sample.
[b] R = resolved; U = unresolved.
[c] Transformation of magnitudes to H-band assumes $V - H = 3.0$, $R - H = 2.5$, $H - K = 0.2$, and $J - H = 0.9$ for the hosts and $H - K = 1$ for the nucleus.

In all cases, the upper limits to the host magnitudes are fainter than $M_H = -26.4$. If the mean value is calculated using only the resolved hosts, we are biased against the faint part of the population and slightly overestimate the luminosity.

3.1. Luminosities and sizes of the host galaxies

In Table 3, we present a comparison of the average host properties of our RQQ sample to those of other previous studies on RQQ, SSRQ, and FSRQ hosts at similar, lower, and higher redshifts. To treat these data homogeneously, the apparent magnitudes reported in each literature study were transformed into absolute H-band magnitudes in our adopted cosmology, after K-correction and color correction, assuming average rest-frame colors for giant ellipticals of $H - K = 0.2$ (Recillas-Cruz et al. 1990), $R - K = 2.7$ (K98), and $J - H = 0.9$ and $V - H = 3.0$ (K00).

According to the AGN unified models (Urry & Padovani 1995), FSRQs are strongly beamed objects, and to avoid any bias due to the contamination from beaming (by an unknown factor) of the nuclear luminosities of the FSRQs, we mainly compare the results for RQQs with those for SSRQs. Figure 3 shows the distribution of the RQQ, SSRQ, and FSRQ host galaxy absolute H-band magnitudes (this work, K00 and K98, respectively) in the redshift range $0.5 < z < 1$. The average absolute magnitude of the 12 resolved RQQ hosts is $M_H = -26.3 \pm 0.6$, and including the three upper limits, $M_H^{all} = -26.2 \pm 0.6$ for the full sample of 15 RQQs. To estimate the total dispersion we used the equation for the variance and added that value to the dispersion of the resolved observations. All the observed RQQs have host galaxies with luminosity ranging between M_H^* and $M_H^* - 2$, where $M_H^* = -25.0$ (Mobasher et al. 1993) is the characteristic luminosity of the Schechter luminosity function for elliptical galaxies. RQQ hosts belong, therefore, preferentially to the high luminosity tail of the galaxy luminosity function. Note that the intermediate redshift RQQ hosts are on average ∼1 mag fainter than SSRQ hosts ($M_H = -27.0 \pm 1.2$) in the same redshift range, even though the nuclear absolute magnitudes of the two samples are similar ($M_H = -27.9 \pm 1.0$ and $M_H = -28.3 \pm 1.3$ for RQQs and SSRQs, respectively). This difference is due to a tail of high luminosity SSRQ hosts ($M_H > -27$) that are not present among the RQQ hosts. A similar difference between the luminosities of RQQ and RLQ hosts has been found in previous studies of quasars at both lower (Dunlop et al. 2003) and higher redshifts (Kukula et al. 2001; Falomo et al. 2004; Kotilainen et al. 2006). For our intermediate redshift RQQ and RLQ samples, selection effects due to, e.g., non-homogeneous distribution in redshift, optical luminosity, and/or modeling of the host galaxy are irrelevant. Our results, therefore, strengthen the conclusion from previous studies that the gap in the host luminosity is intrinsic and remains the same over a wide redshift range between $z = 0$ and $z = 2$. Note that if the host luminosity is related to the bulge mass and thus to the BH mass, and on average RLQ hosts are brighter than RQQ hosts, the BHs in RLQs must be more massive than those in RQQs. Furthermore, to produce a similar optical luminosity, the BHs in RLQs must also be accreting less efficiently than the BHs in RQQs.

Figure 4 shows the average H-band absolute magnitudes derived from the various samples of RQQ host galaxies (Table 3) as a function of redshift, based on NIR HST and ground-based

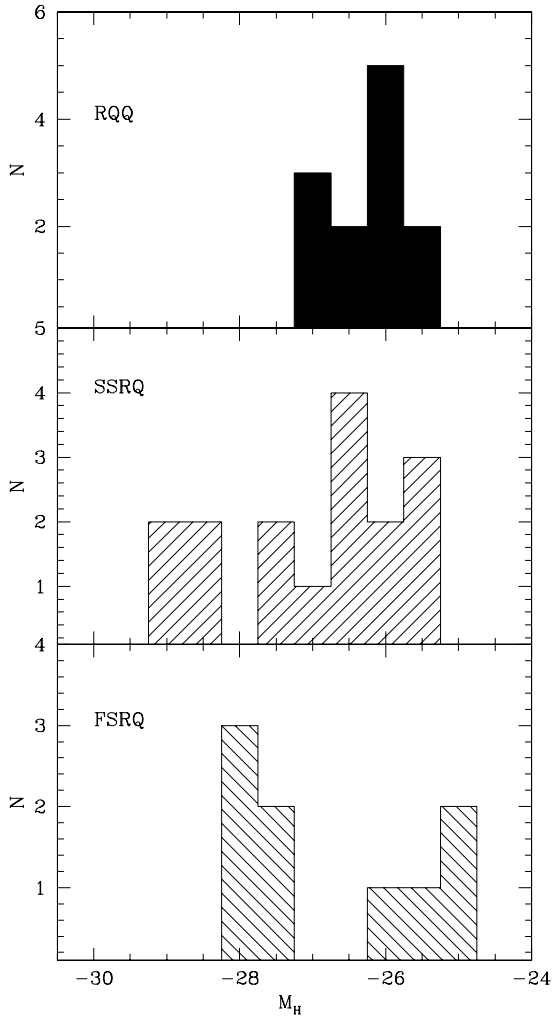

Fig. 3. Histogram of the absolute H-band magnitude of the 12 RQQ hosts (*top*; this work), 16 SSRQ hosts (*middle*; K00), and 9 FSRQ hosts (*bottom*; K98) at the redshift range $0.5 < z < 1$.

data (for explanation of symbols, see the caption of Fig. 4). All these data have been made consistent with our system (as regards extinction, K-correction, and cosmology), starting from the total apparent magnitudes of the host galaxies. Note that at $z < 0.5$ the scatter of the average host galaxy magnitudes between the various samples is much larger than that at higher redshift. Notably, the average host galaxy magnitudes of the low redshift RQQs observed by McLeod & Rieke (1994a), Bahcall et al. (1997), and Percival et al. (2001) are ∼0.5−1 mag fainter than those of the majority of the low redshift RQQ samples. If there is a correlation between nuclear and host luminosities (see next section), the low luminosity RQQs observed by McLeod & Rieke (1994a) (open hexagon) are indeed expected to have relatively low luminosity hosts, confirmed by comparing with their high luminosity RQQ sample (McLeod & Rieke 1994b) (filled hexagon). The case of the discrepant value from the high nuclear luminosity RQQ sample of Percival et al. (2001) is more difficult to interpret. In the host galaxy fitting, they used a varying β parameter, including several cases with a pure exponential disk model, leading to significantly lower host magnitudes than those with an elliptical galaxy model. Furthermore, from their reported data it is not possible to ascertain the data quality (e.g., no luminosity profiles were shown).

Overall, the intermediate redshift RQQ hosts follow the same trend as RQQ hosts at lower and higher redshift. They are consistent with a passive stellar population evolution of massive ellipticals, in the redshift range $0 < z < 2$. This scenario of a passive evolution of quasar hosts agrees with the few available spectroscopic studies of low redshift quasar hosts (Canalizo & Stockton 2000; Nolan et al. 2001), indicating that their stellar content is dominated by an old evolved stellar population. The cosmic evolution traced by quasar hosts up to $z \sim 2$ disagrees with semianalytic hierarchical models of AGN and galaxy formation and evolution (Kauffmann & Hähnelt 2000), which predict fainter (less massive) hosts at high redshift, which merge and grow to form the low redshift massive spheroids. Thus, if quasar hosts are luminous spheroids undergoing passive evolution, their mass remains essentially unchanged from $z \sim 2$ up to the present epoch.

The average effective radius of the 12 resolved intermediate redshift RQQ hosts is $R_e = 11.3 \pm 5.8$ kpc. This is in good agreement with intermediate redshift SSRQ and FSRQ hosts for which $R_e = 8.6 \pm 1.9$ and $R_e = 12.8 \pm 6.0$ kpc, (K00; K98, respectively). The quoted uncertainties are due to the dispersion of the distribution, while the individual large dispersions due to the degeneracy between the effective radius R_e and the surface brightness μ_e have not been taken into account. The intermediate redshift RQQ hosts also have similar sizes to those of both lower redshift RQQ hosts, e.g., $R_e = 11.4 \pm 1.7$ kpc (Dunlop et al. 2003) and $R_e = 8.7 \pm 1.8$ kpc (Floyd et al. 2004), and to those of higher redshift RQQ hosts, e.g., $R_e = 11.6 \pm 2.5$ kpc (Falomo et al. 2004) and $R_e = 6.5 \pm 1.6$ kpc (Kotilainen et al. 2006). This confirms that the effective radius of RQQ hosts does not evolve with redshift, and suggests that at redshift $z > 0.5$, the RQQ hosts have dynamical structures similar to normal (presently inactive) elliptical galaxies.

3.2. Correlation between nuclear and host luminosity

The absolute magnitudes of the nuclear component in the intermediate redshift RQQs range from $M_H \sim -26$ to $M_H \sim -29.5$, with an average value of $M_H = -27.9 \pm 1.0$, in good agreement with that of the average nuclear magnitude of SSRQs ($M_H = -28.3 \pm 1.3$; K00). On the other hand, the nuclear component of the FSRQs is much brighter, $M_H = -29.7 \pm 0.8$ (K98), consistent with their nuclear emission being boosted by relativistic beaming. If the mass of the central BH is proportional to the luminosity of the spheroid of the host galaxy, as observed for nearby massive early-type galaxies, and if the quasar is emitting at a fixed fraction of the Eddington luminosity, one would expect a correlation between the luminosity of the nucleus and that of the host galaxy. However, nuclear obscuration, beaming, and/or an intrinsic spread in accretion rate and mass-to-luminosity conversion efficiency may destroy this correlation. Our combined sample (this work; K00 and K98) covers a broad range of nuclear luminosity ($-24 < M_B < -27$) and can therefore be used to investigate this issue.

Figure 5 shows the H-band absolute host galaxy magnitude versus the absolute nuclear magnitude for intermediate redshift RQQs (this work), FSRQs, and SSRQs (K98; K00, respectively). As noted in the previous section, the intermediate redshift RQQs tend to occupy a region of less luminous host galaxies than the SSRQs. However, before any conclusions are drawn, it is worth noting the obvious selection effects that could introduce a spurious apparent correlation between the nuclear and host luminosities. In particular, two such effects may combine to depopulate the $M_{nuc} - M_{host}$ plane in opposite directions. Firstly,

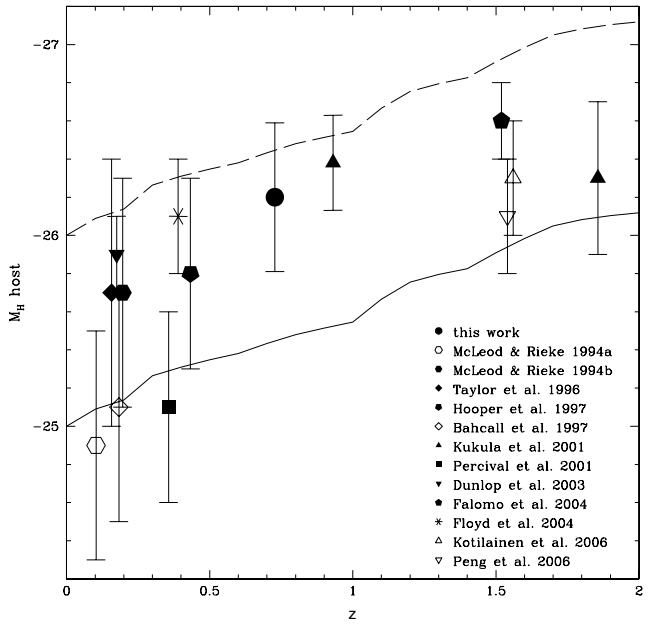

Fig. 4. The average absolute H-band magnitude of RQQ host galaxies as a function of redshift. The combined sample of resolved and unresolved RQQs (this work) is marked as filled circles, the sample from Kukula et al. (2001) as triangles, that from Dunlop et al. (2003) as inverted triangles, that from Percival et al. (2001) as squares, that from Falomo et al. (2004) as pentagons, that from Floyd et al. (2004) as asterisks, that from McLeod & Rieke (1994a,b) as open and filled hexagons, that from Taylor et al. (1996) as diamonds, that from Hooper et al. (1997) as inverted pentagons, that from Bahcall et al. (1997) as open diamonds, that from Kotilainen et al. (2006) as open triangles and that from Peng et al. (2006) as inverted open triangles. The solid and long-dashed lines are the luminosities of L^* ($M_{\rm H} = -25.0$ at low redshift; Mobasher et al. 1993) and $L^* - 1$ galaxies following the passive evolution model of Bressan et al. (1998).

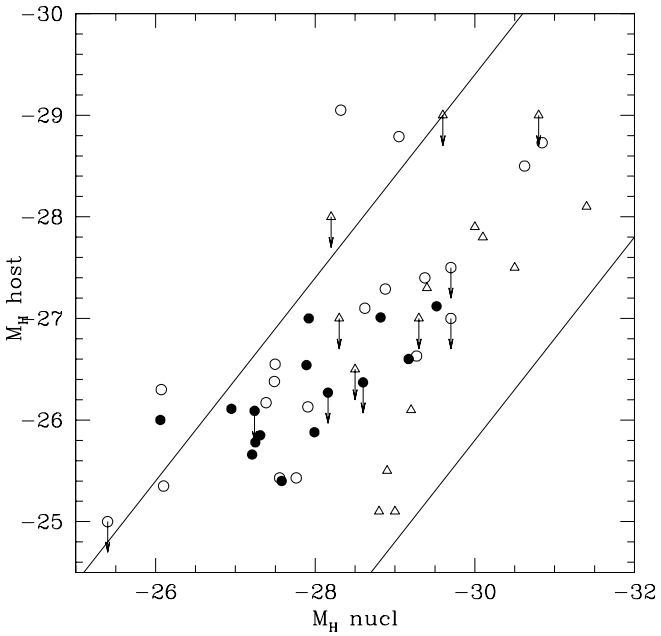

Fig. 5. The H-band absolute magnitude of the nucleus compared with that of the host galaxy. RQQs from this work are marked as filled circles, while SSRQs from K00 and FSRQs from Kotilainen et al. (1998) are marked as open circles and open triangles, respectively. The arrows represent the upper limits of the host luminosity for unresolved objects. The diagonal lines represent the loci of the constant ratio between host and nuclear emission. These can be translated into Eddington ratios assuming that the central black hole mass – galaxy luminosity correlation holds at high redshifts and that the observed nuclear power is proportional to the bolometric emission. The diagonal lines encompass a spread of 1.5 dex in the nucleus/host luminosity ratio.

a faint host would be very difficult to detect against a bright nucleus (upper left hand region). Secondly, a low luminosity nucleus would be difficult to detect against a bright host galaxy (lower-right hand region). In our sample, the first effect should not be very serious because only three RQQs remained unresolved and their upper limits do not populate an extreme region of the diagram. The second effect is likely to be small because of the rareness of extremely luminous galaxies.

We find a reasonably strong nuclear luminosity dependence of the host galaxy luminosity for the full sample of quasars (RQQs and SSRQs), with a Spearman rank correlation coefficient $R_{\rm S} = 0.737$. This correlation is also present when considering the RQQs and SSRQs separately ($R_{\rm S} = 0.606$ and $R_{\rm S} = 0.713$, respectively). The RLQs and RQQs in our study have a similar distribution in their nuclear luminosity, and thus we believe this to be a robust result. Note that we have found a similar dependence at an even higher redshift for RLQs, and to a lesser extent for RQQs (Kotilainen et al. 2006). Since generally no such correlation has been found at low redshift (e.g., Dunlop et al. 2003; Pagani et al. 2003), (but see, e.g., Sanchez et al. (2004), who found a correlation for low luminosity AGN), it must have its onset at a relatively high redshift. Note that the correlation suggests that the low redshift relation between $M_{\rm BH}$ and $M_{\rm bulge}$ also holds at high redshift, but its confirmation requires a spectroscopic determination of BH masses in high redshift quasars. Note also that there is a large scatter in the relationship, possibly due to varying accretion efficiency, and intrinsic scatter in the $M_{\rm BH}-M_{\rm bulge}$ relation.

Assuming that the the H-band nuclear luminosity is proportional to the bolometric luminosity and that the host galaxy luminosity is proportional to the BH mass (as observed at low redshift), the nucleus/host luminosity ratio should be proportional to the Eddington factor $L/L_{\rm E}$, where $L_{\rm E} = 1.25\times10^{38}\times(M_{\rm BH}/M_\odot)$. Figure 6 shows the distribution of the H-band nucleus/host luminosity ratio for the samples of resolved RQQs, FSRQs, and SSRQs. The spread in the nucleus/host luminosity ratio for RQQs is similar to that of SSRQs, but smaller than that of FSRQs. For the resolved intermediate redshift RQQs, the average H-band nucleus/host ratio is $\log(L_{\rm nuc}/L_{\rm host}) = 0.71 \pm 0.29$, slightly higher than that in intermediate redshift SSRQs ($\log(L_{\rm nuc}/L_{\rm host}) = 0.58 \pm 0.51$), but lower than that in the FSRQs ($\log(L_{\rm nuc}/L_{\rm host}) = 1.32 \pm 1.04$), consistent with the idea that the nuclear luminosities of the FSRQs are affected by strong nuclear beaming. The nucleus/host ratio of intermediate redshift RQQs is lower than that found for higher redshift high luminosity RQQs with $\log(L_{\rm nuc}/L_{\rm host}) = 1.32 \pm 0.37$ (Falomo et al. 2004), but is consistent with the ratio observed for high redshift low luminosity RQQs with $\log(L_{\rm nuc}/L_{\rm host}) = 1.00 \pm 0.44$ (Kotilainen et al. 2006) and $\log(L_{\rm nuc}/L_{\rm host}) = 0.61\pm0.69$ (Kukula et al. 2001). Thus, $L/L_{\rm E}$ appears to depend on quasar luminosity, being significantly higher in high luminosity quasars (see Kotilainen et al. 2006). This may indicate a smaller accretion efficiency in low luminosity quasars.

Assuming that the R-band host galaxy luminosity is proportional to the BH mass, we can estimate the BH mass for each resolved RQQ using the relation $\log(M_{\rm bh}/M_\odot) = -0.50(\pm0.02)M_{\rm R} - 2.96(\pm0.48)$ (McLure & Dunlop 2002; Marconi & Hunt 2003). We have used $R - K = 2.7$ (K98)

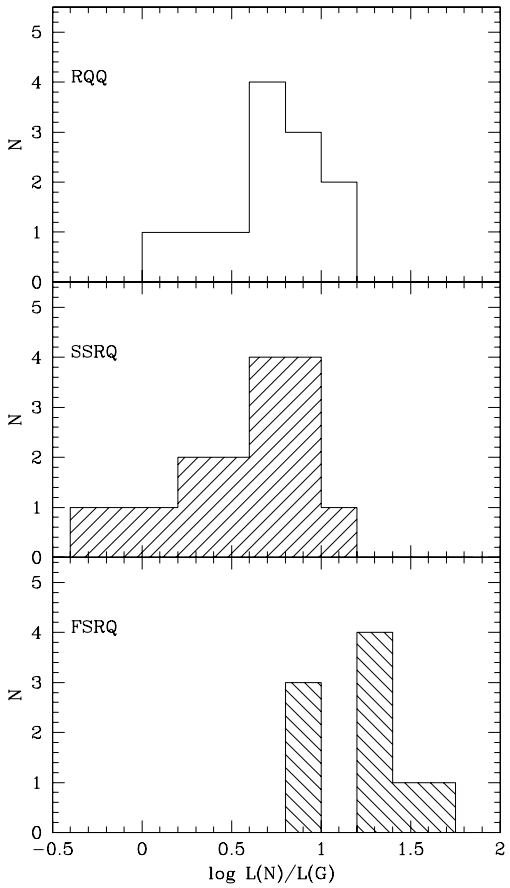

Fig. 6. Histogram of the nucleus/host luminosity ratio for the resolved RQQs (*top*), SSRQs (*middle*; K00), and FSRQs (*bottom*; K98).

and $H - K = 0.2$ (Recillas-Cruz et al. 1990) to transform the H-band magnitudes to the R-band. The resulting BH masses are given in Table 4. The average value for the BH masses of RQQs is $M_{\rm BH,RQQ} = 1.0 \pm 0.6 \times 10^9\ M_\odot$, with five out of the 12 RQQs having BH masses above $10^9\ M_\odot$. This is consistent with the average BH mass for low redshift RQQs, $M_{\rm BH,RQQ} = 1.05 \pm 0.24 \times 10^9\ M_\odot$ (Dunlop et al. 2003). These values can be compared with the BH masses of the intermediate redshift RLQs, $M_{\rm BH,RLQ} = 4.1 \pm 5.6 \times 10^9\ M_\odot$ (K98; K00). The BH masses of the RLQs thus seem to be about four times larger than the BH masses of the RQQs. This may reflect a fundamental difference between RQQs and RLQs and supports the idea that the radio properties of quasars depend on the mass of the central BH.

3.3. The close environments of RQQs

Quasars often have close companions, and their host galaxies sometimes exhibit a disturbed morphology (e.g., Yee & Green 1984; Stockton & MacKenty 1987; Hutchings & Neff 1990; Hutchings 1995; Bahcall et al. 1997; Hutchings et al. 1999). Spectroscopic studies (e.g., Heckman et al. 1984; Canalizo & Stocton 1997) have shown that indeed in many cases the companions are at the redshift of the quasar and are therefore physically associated. This is consistent with the long-standing idea that strong tidal interactions and galaxy mergers can trigger and/or fuel the nuclear activity.

Both RLQs and RQQs seem to inhabit relatively dense environments (e.g., groups of galaxies), but are only rarely located in rich galaxy clusters. Although some earlier studies suggested that RQQs are generally found in poorer environments than RLQs (e.g., Ellingson et al. 1991), the majority of recent studies (e.g., Wold et al. 2000, 2001; McLure & Dunlop 2001) have come to the conclusion that there is no significant difference between the large scale environments of RQQs and RLQs. Clarifying this issue is important for understanding the connection between the characteristics of the nuclear activity (e.g., the level of nuclear radio emission) and the environment.

Following the method in K00, we have compared the frequency of companions found around the samples of RQQs and RLQs at intermediate z discussed in the previous sections. For each RQQ, we counted the number of resolved companion objects, i.e., galaxies, within a specified radius that are brighter than $m^*_{\rm H} + 2$, where $m^*_{\rm H}$ is the apparent magnitude corresponding to $M^*_{\rm H} = -25$ at the redshift of each quasar. This limit is in all cases at least 1 mag brighter than the magnitude limit of the images. We selected two radii corresponding to projected distances of 50 kpc and 100 kpc around the quasar. In our adopted cosmology, 50 kpc corresponds to ∼5.3 arcsec and 100 kpc to ∼10.6 arcsec at the average redshift of the samples, $z \sim 0.7$.

Table 4. The black hole masses of the RQQs[a].

Object	$M_{\rm BH}/10^9\ M_\odot$
HS 0010+3611	0.5
1E 0112+3256	1.3
PB 6708	<0.7
KUV 03086-0447	2.0
US 3828	0.5
MS 08287+6614	0.7
TON 392	1.3
US 971	0.4
HE 0955-0009	<0.9
HE 1100-1109	2.2
CSO 769	1.1
HS 1623+7313	0.3
HS 2138+1313	<1.0
LBQS 2249-0154	1.2
ZC 2351+010B	0.5

[a] Transformations of magnitudes to R-band done assuming $R-H = 2.5$.

Table 5. The close environments of the RQQs[a].

Name	z	$N_{\rm r}$ (50 kpc)	$N_{\rm r}$ (100 kpc)
HS 0010+3611	0.530	0	0
1E 0112+3256	0.764	0	1
PB 6708	0.868	1	1
KUV 03086-0447	0.755	0	0
US 3828	0.515	1	1
MS 08287+6614	0.610	0	1
TON 392	0.654	0	1
US 971	0.703	0	0
HE 0955-0009	0.597	0	0
HE 1100-1109	0.994	0	3
CSO 769	0.850	0	0
HS 1623+7313	0.621	0	0
HS 2138+1313	0.810	2	3
LBQS 2249-0154	0.832	0	2
ZC 2351+010B	0.810	0	1

[a] Column (1) gives the name of the object; (2) the redshift of the object; (3) the number of companions within 50 kpc radius; (4) the number of companions within 100 kpc radius.

Table 6. Close companions of RQQs and RLQs[a].

Sample	N_{ave} (50 kpc)	N_{ave} (100 kpc)	N_c/N_{tot} (50 kpc)	N_c/N_{tot} (100 kpc)
RQQ (this work)	0.27 ± 0.59	0.93 ± 1.03	20%	60%
FSRQ (K98)	0.19 ± 0.39	1.19 ± 1.01	19%	75%
SSRQ (K00)	0.05 ± 0.22	0.53 ± 0.68	5%	42%

[a] Column (1) gives the sample; (2) the average number of companions within 50 kpc radius; (3) the average number of companions within 100 kpc radius; (4) and (5) the fraction of quasars with close companion within 50 kpc and 100 kpc radius, respectively.

In Table 5 we give the number of resolved companions (N_r) within 50 and 100 kpc projected distance from each RQQ.

The average number of companions around the RQQs (this work), FSRQs, and SSRQs (K98; K00, respectively) are reported in Table 6, together with the fraction of quasars that have at least one close companion. RQQs appears to inhabit environments similar to FSRQs, but richer than SSRQs. It seems that there is not a direct link with radio properties between RQQs and RLQs which is consistent with the results by Smith et al. (2000),Wold et al. (2001) and McLure & Dunlop (2001). From our results it appears that neither RQQs nor RLQs have significant numbers of close companions to be important for the triggering and fueling of nuclear activity. However, it remains a possibility that the timescales of the interaction and the triggering are so different that by the time of the onset of the nuclear activity, no detectable sign of the past interaction remains.

4. Conclusions

We have presented a near-infrared imaging study of a sample of radio-quiet quasars at $0.5 < z < 1$. In 12 out of the 15 quasars observed, we were able to resolve the objects and to characterize the properties of their host galaxies. The RQQ host galaxies at $z \sim 0.7$ are luminous elliptical galaxies, with average magnitude $M_H = -26.3 \pm 0.6$, ∼1 mag brighter than low redshift L^* galaxies. Our results are consistent with the passively evolving stellar population that was created at high redshift ($z \sim 3-4$). RQQ hosts are ∼0.5 magnitudes fainter than those of RLQs at all redshifts in the range $0 < z < 2$. The host galaxies of the intermediate redshift RQQs are giant ellipticals, with an average effective radius $R_e = 11.3 \pm 5.8$ kpc. This is similar to those of lower and higher redshift RQQs, indicating that the effective radius of the host galaxies does not evolve with redshift. The intermediate redshift RQQs tend to have fainter nuclear luminosity than FSRQs and SSRQs at the same redshift, suggesting that their central engine is less powerful. RQQs have relatively rich environments, similar to the environments of FSRQs.

Acknowledgements. T.H., J.K.K., and E.Ö. acknowledge financial support from the Academy of Finland, projects 8107775 and 8201017. This work has been partially supported by INAF contract 1301/01.

References

Aragon-Salamanca, A., Baughand, C., & Kauffmann, G. 1998, MNRAS, 297, 427
Bahcall, J., Kirhakos, S., Saxe, D., & Schneider, D. 1997, ApJ, 479, 642
Barger, A., Cowie, L., Bautz, M., et al. 2001, AJ, 122, 2177
Barth, A. 2004, in The Interplay among Black Holes, Stars and ISM in Galactic Nuclei, ed. L. H. T. Storchi-Bergmann, & H. R. S. C. UK (Cambridge University Press), 3
Becker, R., Helfand, D., White, R., Gregg, M., & Laurent-Muehleisen, S. 1997, ApJ, 475, 479
Bettoni, D., Falomo, R., Fasano, G., & Govoni, F. 2003, A&A, 399, 869
Bressan, A., Granato, G., & Silva, L. 1998, A&A, 332, 135
Canalizo, G., & Stockton, A. 2000, ApJ, 528, 201
Canalizo, G., & Stocton, A. 1997, ApJ, 480, L5
Chary, R., & Elbaz, D. 2001, ApJ, 556, 562
Di Matteo, T., Croft, R., Springel, V., & Hernquist, L. 2003, ApJ, 593, 56
Dunlop, J., McLure, R., Kukula, M., et al. 2003, MNRAS, 340, 1095
Ellingson, E., Yee, H., & Green, R. 1991, ApJ, 371, 49
Falomo, R., Kotilainen, J., Pagani, C., Scarpa, R., & Treves, A. 2004, ApJ, 604, 495
Falomo, R., Kotilainen, J., Scarpa, R., Treves, A., & Uslenghi, M. 2006, A&A, submitted
Falomo, R., Kotilainen, J., & Treves, A. 2001, ApJ, 547, 124
Feigelson, E., & Nelson, P. 1985, ApJ, 293, 192
Ferrarese, L. 2002, in Proceedings of the 2nd KIAS Asrtophysical Workshop, ed. L. C.-H., & C. H.-Y. (Singapore: World scientific Publishing), 3
Ferrarese, L., & Merritt, D. 2000, ApJ, 539, L9
Floyd, D., Kukula, M., Dunlop, J., McLure, R., & Miller, L. 2004, MNRAS, 355, 196
Franceschini, A., Hasinger, G., Miyaji, T., & Malquori, D. 1999, MNRAS, 310, L5
Gebhardt, K., Bender, R., Bower, G., Dressler, A., & Faber, S. 2000, ApJ, 539, L13
Hamilton, T., Casertano, S., & Turnshek, D. 2002, ApJ, 576, 61
Häring, N., & Rix, H. 2004, ApJ, 604, L89
Heckman, T., Bothun, G., Balick, B., & Smith, E. 1984, AJ, 89, 958
Hooper, E., Impey, C., & Foltz, C. 1997, ApJ, 480, L95
Hunt, L., Mannucci, F., Testi, L., et al. 1998, AJ, 115, 2594
Hutchings, J. 1995, AJ, 110, 994
Hutchings, J., & Neff, S. 1990, AJ, 99, 1715
Hutchings, J., Crampton, D., Morris, S., Durand, D., & Steinbring, E. 1999, AJ, 117, 1109
Kauffmann, G., & Hähnelt, M. 2000, MNRAS, 311, 576
Kotilainen, J., & Falomo, R. 2000, A&A, 364, 70
Kotilainen, J., Falomo, R., & Scarpa, R. 1998, A&A, 332, 503
Kotilainen, J., Hyvönen, T., & Falomo, R. 2005, A&A, 440, 831
Kotilainen, J., Falomo, R., Labita, M., Treves, A., & Uslenghi, M. 2006, ApJ, submitted
Kukula, M., Dunlop, J., McLure, R., et al. 2001, MNRAS, 326, 1533
Madau, P., Pozzetti, L., & Dickinson, M. 1998, ApJ, 498, 106
Magorrian, J., Tremaine, S., Richstone, D., et al. 1998, AJ, 115, 2285
Marconi, A., & Hunt, L. 2003, ApJ, 589, L21
Marconi, A., Risaliti, G., Gilli, R., et al. 2004, MNRAS, 351, 169
McLeod, K., & Rieke, G. 1994a, ApJ, 420, 58
McLeod, K., & Rieke, G. 1994b, ApJ, 431, 137
McLure, R., & Dunlop, J. 2001, MNRAS, 321, 515
McLure, R., & Dunlop, J. 2002, MNRAS, 331, 795
Mobasher, B., Sharples, R., & Ellis, R. 1993, MNRAS, 263, 560
Neugebauer, G., Matthews, K., Soifer, B., & Elias, J. 1985, ApJ, 298, 275
Nolan, L., Dunlop, J., Kukula, M., Hughes, D., & Boroson, T. 2001, MNRAS, 323, 308
Pagani, C., Falomo, R., & Treves, A. 2003, ApJ, 596, 830
Peng, C., Impey, C., Rix, H.-W., et al. 2006 [arXiv:astro-ph/0603248]
Percival, W., Miller, L., McLure, R., & Dunlop, J. 2001, MNRAS, 322, 843
Recillas-Cruz, E., Carrasco, L., Serrano, A., & Cruz-Gonzalez, I. 1990, A&A, 229, 64
Sanchez, S., Jahnke, K., Wisotzki, L., et al. 2004, ApJ, 614, 586
Smith, R., Boyle, B., & Maddox, S. 2000, MNRAS, 313, 252
Stockton, A., & MacKenty, J. 1987, ApJ, 316, 584
Taylor, G., Dunlop, J., Hughes, D., & Robson, E. 1996, MNRAS, 283, 930
Thuan, T., & Puschell, J. 1989, ApJ, 346, 34
Urry, C., & Padovani, P. 1995, PASP, 107, 803
van der Marel, R. 1999, AJ, 117, 744
Veron-Cetty, M., & Veron, P. 2003, A&A, 412, 399
Warren, S., Hewett, P., & Osmer, P. 1994, ApJ, 421, 412
Wold, M., Lacy, M., Lilje, P., & Serjeant, S. 2000, MNRAS, 316, 267
Wold, M., Lacy, M., Lilje, P., & Serjeant, S. 2001, MNRAS, 323, 231
Yee, H., & Green, R. 1984, ApJ, 280, 79
Yu, Q., & Tremaine, S. 2002, MNRAS, 335, 965

Online Material

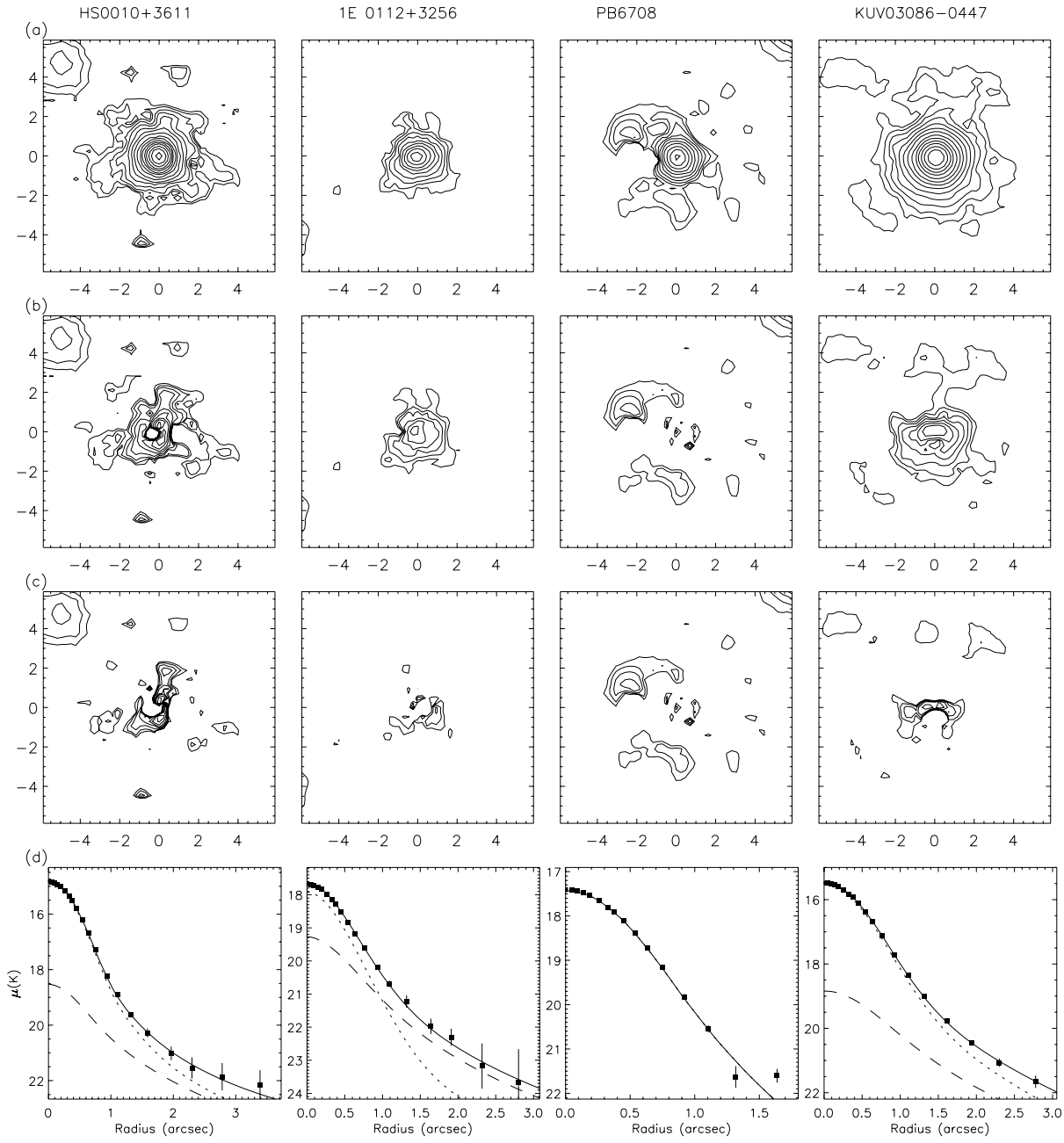

Fig. 2. The *H*-band images of the quasars, from *top* to *bottom* **a)** the original image, **b)** the PSF model subtracted image of the host galaxy, and **c)** residuals after the model fitting. Panel **d)** shows the observed radial surface brightness profiles (solid points with error bars) for each quasar, overlaid with the scaled PSF model (dotted line), the de Vaucouleurs $r^{1/4}$ model convolved with the PSF (long-dashed line), and the fitted PSF + host galaxy model profile (solid line). The *Y*-axis is in mag arcsec^{-2}.

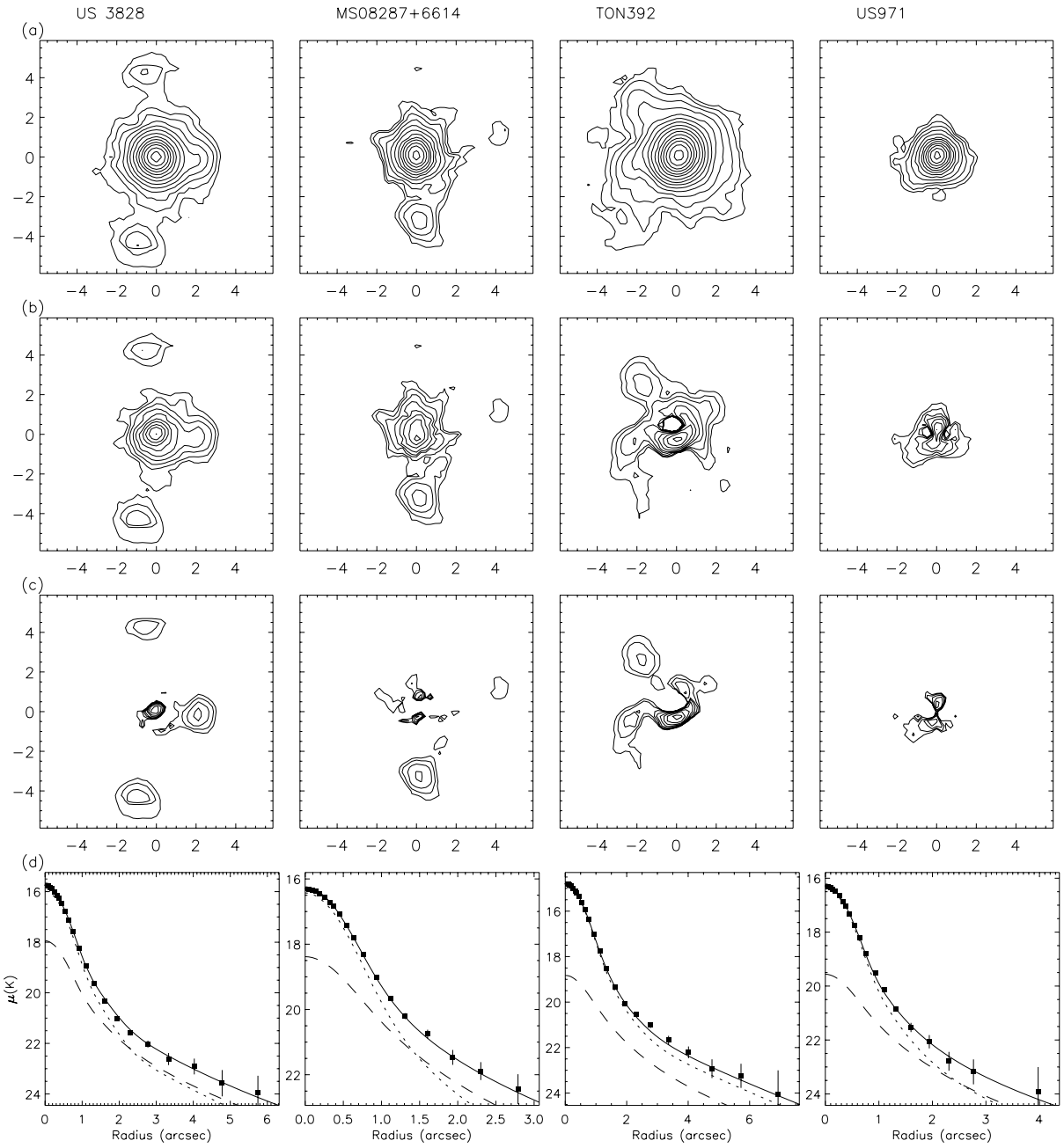

Fig. 2. continued.

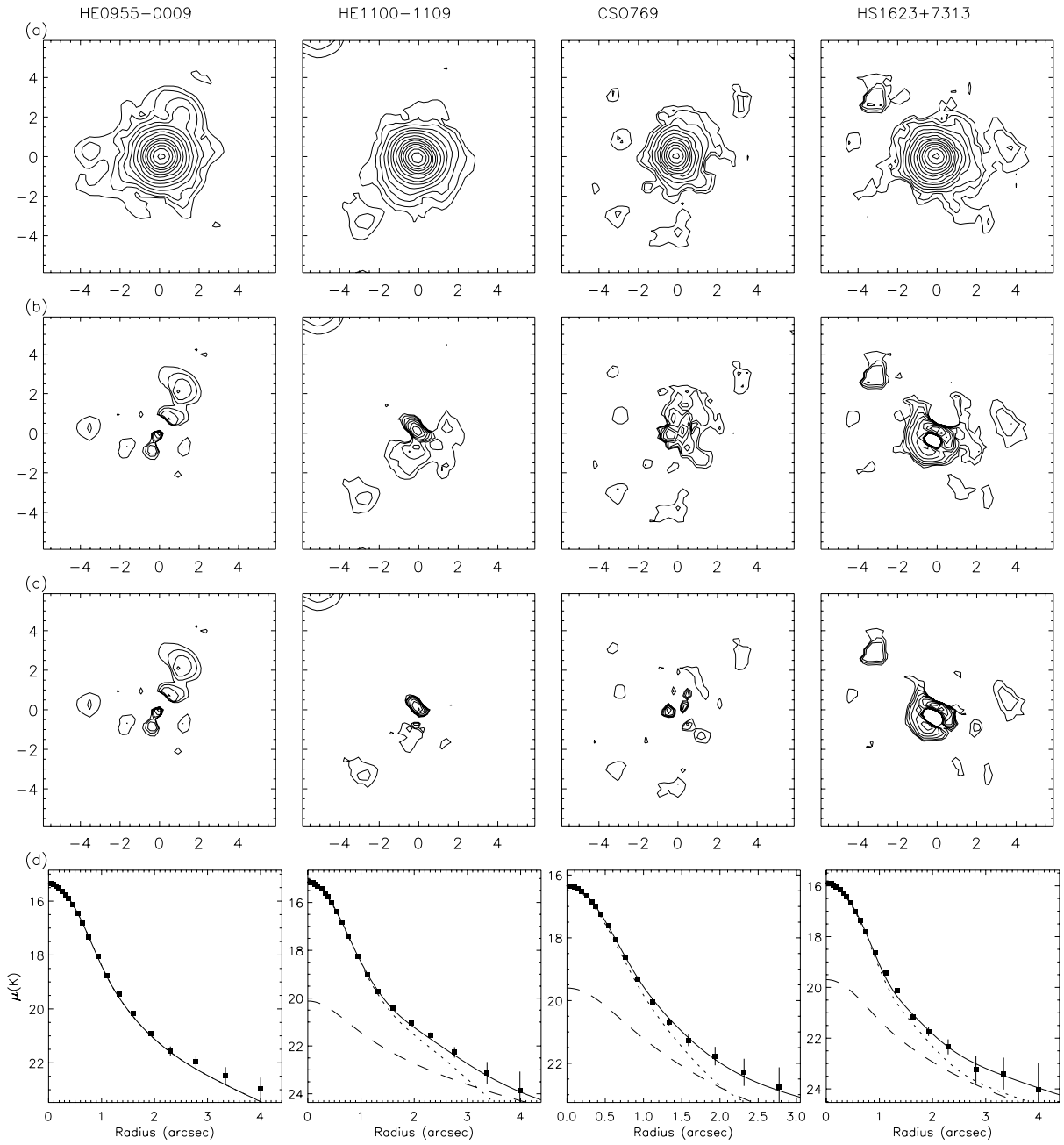

Fig. 2. continued.

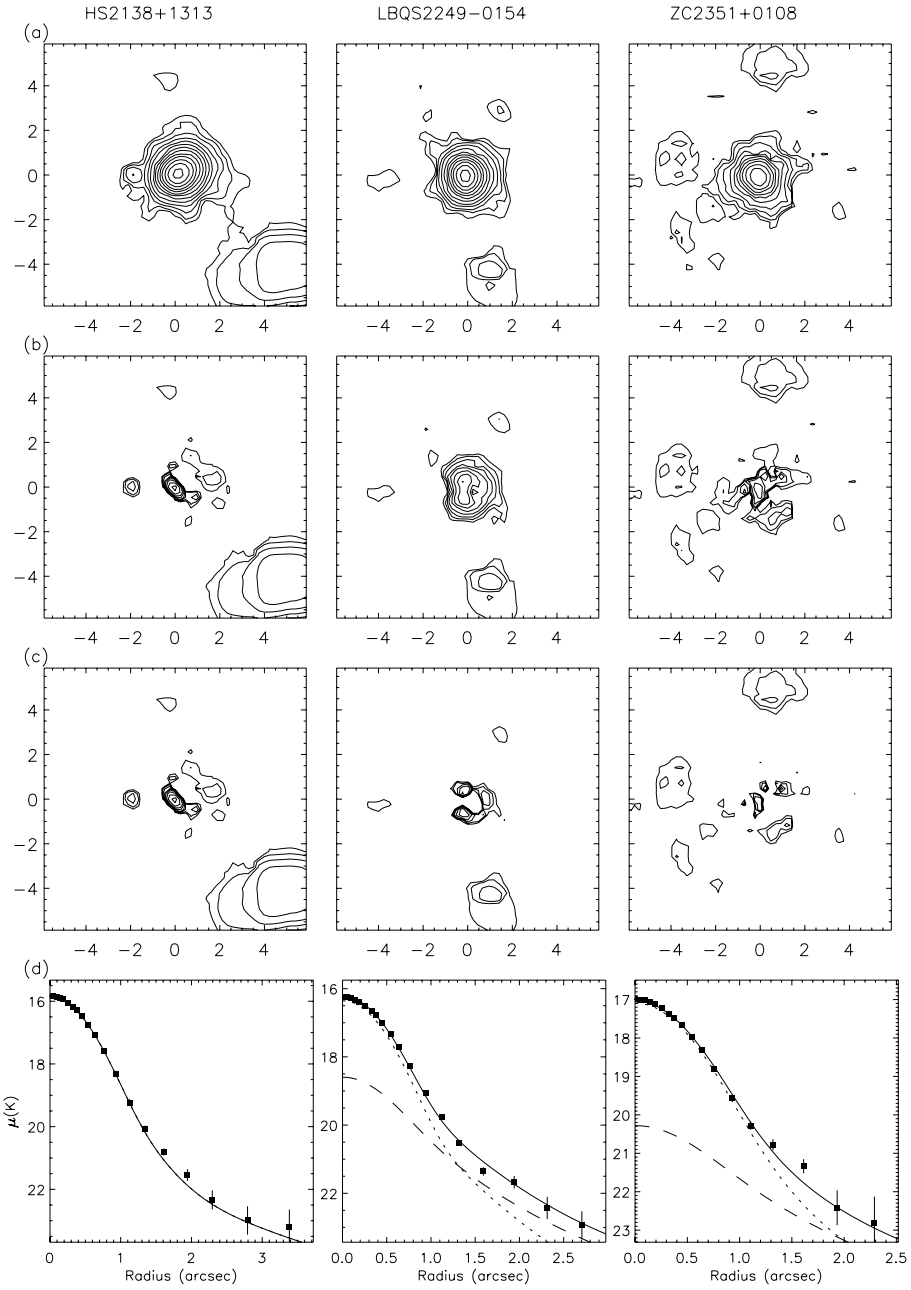

Fig. 2. continued.